recycling

MDPI

Article

Effect of Pretreatment on the Structure and Enzymatic Hydrolysis of Pineapple Waste Biomass in Hydrothermal Deconstruction

Carlos Méndez-Durazno [1], Nilo M. Robles Carrillo [2,3], Valeria Ramírez [2], Oscar M. Rodriguez-Narváez [4], Pablo A. Cisneros-Pérez [5], Diego Chulde [2], Alexis Debut [6] and Patricio J. Espinoza-Montero [1,*]

1 Escuela de Ciencias Químicas, Pontificia Universidad Católica del Ecuador, Quito 170525, Ecuador; camendezd@puce.edu.ec
2 Instituto de Investigación Geológico y Energético IIGE, Quito 170518, Ecuador; nilo.robles@geoenergia.gob.ec (N.M.R.C.); valeria_1304@hotmail.com (V.R.); diego.chulde@geoenergia.gob.ec (D.C.)
3 Alimentos, Compuestos Orgánicos, Materiales, Microbiología Aplicada, Energía (ACMME), Facultad de Ingeniería Química, Universidad Central del Ecuador, Quito 170129, Ecuador
4 Dirección de Investigación y Soluciones Tecnológicas, CIATEC, A.C., Calle Omega 201, Industrial Delta, León 37545, Guanajuato, Mexico; orodriguez@ciatec.mx
5 School of Chemical Sciences and Engineering, Yachay Tech University, Urcuquí 100650, Ecuador; pcisneros@yachaytech.edu.ec
6 Centro de Nanociencia y Nanotecnología, Universidad de las Fuerzas Armadas ESPE, Sangolquí 170501, Ecuador; apdebut@espe.edu.ec
* Correspondence: pespinoza646@puce.edu.ec; Tel.: +593-2299-1700 (ext. 1929)

Abstract

Pineapple biomass represents an abundant renewable source of carbon and a promising feedstock with considerable potential for the production of sustainable fuels. In the present study, the influence of liquid hot water (LHW) pretreatment on the pineapple mother plant was investigated at different controlled severities, then characterized by Fourier-transform infrared spectroscopy (FTIR), X-ray diffraction (XRD), thermogravimetric analysis (TGA), and scanning electron microscopy (SEM). Results show that LHW pretreatment causes structural changes, leading to lignin and hemicellulose depolymerization up to a severity factor of 2.36–3.55, whereas at severity factors in the range of 4.13–5.90, cellulose, hemicellulose, and lignin appear to repolymerize. This pretreatment resulted in a higher hydrolysis efficiency (94.92 ± 0.04%) at 50 °C for 72 h. Compared with the untreated sample, the hydrolysis rate under these conditions increased by a factor of 2.16. SEM imaging revealed significant disruption of the PMP microstructure following LHW treatment, while XRD data confirmed an increase in the crystallinity index. FTIR analysis further indicated modifications in functional group profiles, supporting the structural and compositional changes induced by pretreatment. Overall, this study demonstrates the effectiveness of LHW pretreatment in enhancing the enzymatic digestibility and modifying the physicochemical properties of PMP biomass, providing a foundation for its valorization into high value bioproducts.

Keywords: enzyme hydrolysis; severity factor; liquid hot water treatment; pineapple mother plant

check for updates

Academic Editor: Eugenio Cavallo

Received: 21 June 2025
Revised: 16 October 2025
Accepted: 21 October 2025
Published: 28 October 2025

Citation: Méndez-Durazno, C.; Robles Carrillo, N.M.; Ramírez, V.; Rodriguez-Narváez, O.M.; Cisneros-Pérez, P.A.; Chulde, D.; Debut, A.; Espinoza-Montero, P.J. Effect of Pretreatment on the Structure and Enzymatic Hydrolysis of Pineapple Waste Biomass in Hydrothermal Deconstruction. *Recycling* **2025**, *10*, 198. https://doi.org/10.3390/recycling10060198

Copyright: © 2025 by the authors. Licensee MDPI, Basel, Switzerland. This article is an open access article distributed under the terms and conditions of the Creative Commons Attribution (CC BY) license (https://creativecommons.org/licenses/by/4.0/).

1. Introduction

Rapid urbanization and technological progress have boosted energy consumption and fast-growing anthropogenic CO_2 emissions, leading to a significant environmental

crisis [1,2]. Over the past 60 years, long-running measurements have shown that the CO_2 concentration in the atmosphere has increased by almost 35% [3]. The efficient generation of renewable energy from lignocellulosic biomass (LCB) is a research frontier and a potential pathway to overcome energy demand problems. In this context, LC biomass is considered a promising source of organic carbon that can be converted into chemicals and fuels [4,5]. It has been reported that LCB can deliver 6 MJ of energy, or 0.8 kg of chemicals per kg of feedstock [6]. Currently, the global production of LCB per year has reached a large scale with more than 180 billion tons produced, 94% of which come from agricultural waste [4]. LCB is mainly composed of regions of crystalline and amorphous cellulose microfibrils, dispersed in a dense matrix formed of hemicellulose and lignin [7,8]. Their content, complexity, and spatial interconnections hamper their efficient utilization [9]. The conversion of lignocellulose to valuable products usually comprises two major biochemical reactions: pretreatment and enzyme hydrolysis. Recalcitrance remains a key factor that must be faced before the full potential of the conversion of LCB can be used. The hierarchical structure complexity, lignin and hemicellulose content, degrees of crystallinity and polymerization, and cellulose accessibility contribute to the recalcitrant nature of LCB [10]. Hemicellulose and lignin easily absorb the cellulase through hydrophobic, electrostatic, and hydrogen-bonding interactions, which leads to poor yields of cellulose conversion [11,12]

To address the challenge of cost-effectively converting LCB in bioethanol fermentation, extensive research is currently being undertaken to develop commercially viable LCB pretreatment strategies, including mechanical, chemical, and physico-chemical methods [13]. Among these, hydrothermal pretreatment, also called liquid hot water (LHW), is considered an environmentally friendly processing technology, in terms of cost, availability, and reaction conditions, and is practically more feasible due to the medium only containing feedstock and water, and requiring a short residence time [14,15]. In particular, in this process the hydronium ions released by water autoionization and from in situ generated acids during the pretreatment cause a selective autohydrolisis of glycoside bonds of hemicellulose and partial delignification of the associated lignin, which leads to increased accessibility of cellulose to enzymatic hydrolysis [15–17]. In a previous study, Ruan et al. [18] pretreated sugarcane bagasse under optimal conditions, achieving a cellulose conversion rate of 85.33%.

In particular, pineapple (*Ananas comosus* (L.) *Merr.*) is an important tropical fruit with an annual production of 24.8 million tonnes [19]. After extracting the pulp or fruit, over 80% of the by-products are wasted or discarded improperly [20]. Literature reveals that LHW pretreatment of pineapple leaves at 160 °C provides the highest yield of glucooligosaccharides [21]. Yadav et al. [22] reported that pineapple biomass has low amounts of lignin, which favors the enzymatic hydrolysis of cellulose. Very few studies on using pineapple mother plant (PMP) residue for bioethanol production are available. In this work, pineapple mother plant LHW deconstruction was carried out under different severity conditions. The raw material was subjected to nonisothermal heating in a batch reactor. The changes in the mechanics of raw material cell walls after hydrothermal modification were analyzed in terms of composition, chemical, and morphological structure. Particular attention was paid to the interrelation between severity and enzymatic digestibility The work provides a basis for further study on the conversion of pineapple to second-generation ethanol in biorefineries.

2. Results and Discussion

2.1. Chemical Characterization

The PMP sample comprised 46.27 ± 0.53% cellulose, 17.27 ± 0.34% hemicellulose, and 17.13 ± 0.05% lignin (Table 1). The untreated PMP sample shared common composition

with other LCB such as pineapple leaves (cellulose 59.90 ± 2.10%, hemicellulose 10.88 ± 0.35% and lignin 14.2 ± 0.42%) [23]. To study the effect of SF on the enzymatic hydrolysis of PMP, we performed LHW pretreatment on samples at SF of 2.36 to 5.90 with a residence time of 60 min. The SF during LHW had a strong effect on the chemical composition of PMP; at higher SF, as previously reported, water is most adept to act as a weak acid [24]. A common feature of LHW pretreatment is the cleavage of the glycoside bonds of amorphous cellulose at 150 °C and the progressive degradation of the crystalline portion at 180 °C [24]. The results in Figure 1 and Table 2 illustrate that the cellulose and hemicellulose content decreased as SF increased. Given that cellulose loss occurs at high SF (4.13–5.90), the optimal SF for maximum cellulose conversion was found to be at 3.55. Owing to SF, the hemicellulose depolymerization increased along the LHW pretreatment, as can be observed in Table 2. Delignification confirmed the effect of LHW pretreatment on the chemical composition of PMP. However, during the LHW process, the delignification decreased, in line with the effect of an increase in hemicellulose and cellulose degradation, which contributed to pseudo lignin formation. It was previously reported that the formation of carbohydrate degradation products and their condensation with lignin fragments then accounts for the formation of pseudo lignin [25,26]. From the increase in pseudo lignin content, the enzymatic conversion can be abruptly reduced [27]. Moreover, during the LHW pretreatment, substantial solid recovery reduction was observed, which gradually decreased to 35.11% due to the cellulose and hemicellulose depolymerization. These results are consistent with the reported findings in the literature [28–30].

Table 1. Chemical composition of pineapple mother plant (PMP).

Component	Content (wt% d.w.)
Cellulose	46.27 ± 0.53
Hemicellulose	17.29 ± 0.34
Lignin	17.13 ± 0.05
Extractive free ash	2.96 ± 0.01
Water extractives	13.18 ± 0.37
Ethanol extractives	3.99 ± 0.09
Total extractives	17.17 ± 0.39
Total	100.82

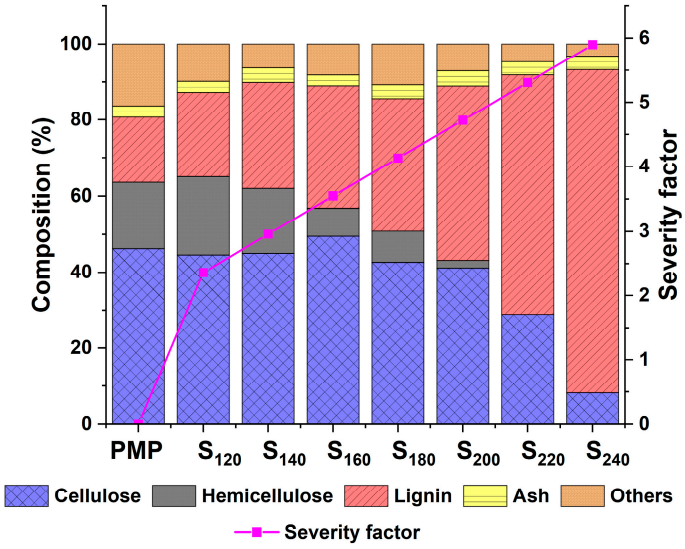


Figure 1. Compositional characterization of solid residues from the LWH-pretreated pineapple mother plant.

Table 2. Chemical composition of LHW treated pineapple mother plant (PMP).

Composition (wt% d.w)	LHW						
	120 °C	**140 °C**	**160 °C**	**180 °C**	**200 °C**	**220 °C**	**240 °C**
Severity factor ($logR_0$)	2.36	2.96	3.55	4.13	4.72	5.31	5.90
Extractive-free ash	2.90 ± 0.03	3.86 ± 0.13	2.87 ± 0.01	3.67 ± 0.03	4.05 ± 0.01	3.51 ± 0.03	3.53 ± 0.01
Lignin	22.18 ± 0.15	27.79 ± 0.01	32.09 ± 0.68	34.73 ± 0.07	45.74 ± 0.15	62.98 ± 0.39	85.08 ± 0.88
Cellulose	44.57 ± 0.83	45.05 ± 1.66	49.53 ± 1.32	42.65 ± 0.97	41.14 ± 0.75	28.87 ± 0.21	8.19 ± 0.32
Hemicellulose	20.49 ± 0.19	16.99 ± 0.40	7.34 ± 0.17	8.21 ± 0.39	2.02 ± 0.10	0	0
Solid recovery	58.19	54.99	51.07	37.29	34.95	30.67	35.11
Cellulose loss	43.95	46.46	45.34	65.63	68.92	80.85	93.78
Hemicellulose loss	31.06	45.99	78.92	82.29	95.92	100	100
Delignification	24.66	10.79	4.34	24.41	6.67	0	0

2.2. FTIR Analysis

ATR-FTIR spectroscopy was recorded to gain insights into the changes in cellulose, hemicellulose, and lignin structure during the sequence of treatments performed on the PMP. The FTIR spectra of the raw material and their LHW pretreatments at increasing SF are shown in Figure 2. The broad band between 3340 and 3270 cm^{-1} was related to the O–H stretching vibrations of alcohols, carboxylic acids, and hydroperoxides [31,32]. Meanwhile, the bands at 2916–2840 cm^{-1} were attributed to the methyl group of alkanes and C-H links. As SF decreased, a significant increase in band intensity at 1730 cm^{-1} was observed, which was attributed to the acetyl and uronic ester groups of the hemicelluloses, evidencing the hemicellulose removal and/or the deacetylation of hemicelluloses. The region around 1060–1030 cm^{-1} shows two weak peaks after LHW pretreatment, suggesting that the hemicellulose content was decreased. Comparisons of FT-IR spectra obtained before and after LHW pretreatment reveal changes in the ester linkage C=O between lignin and hemicellulose, and the C–O–C stretch corresponding to the acetyl group in hemicellulose at 1247 cm^{-1} was significantly reduced.

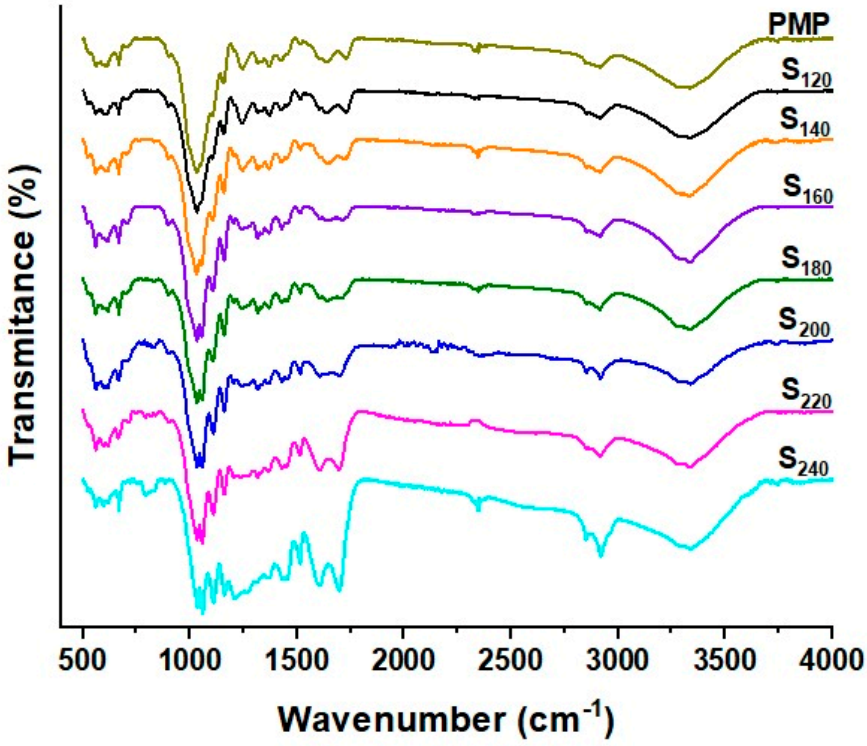


Figure 2. FTIR spectra of the raw PMP and the samples pretreated by different SF.

In contrast, hemicellulose had noticeable changes in the region of 1247 cm^{-1}. The bending mode of adsorbed water was reported to be around 1640 cm^{-1} [33]. C=O stretching vibration can be linked to ketones with a wavenumber between 1636 and 1602 cm^{-1}. Peaks at 1516 and 1424 cm^{-1} represent the skeletal C=C vibrations of aromatic rings in lignin. The band at 1457 cm^{-1} shows the C–H bending or scissoring of alkanes found in pretreated PMP. The 1174 and 1120 cm^{-1} peaks are due to C–O asymmetric bridge stretching. The intensity bands at 1513 cm^{-1} and 1450 cm^{-1} increased considerably after pretreatment, consistent with the increases in lignin content. Based on the FTIR spectrum, there are similarities in the fingerprint region of 1420–670 cm^{-1}, characteristic of lignocellulosic biomass. The absorption lines at 1462 and 2943 cm^{-1} are attributed to the stretching and deformation vibration of C–H bonds in the methyl, methylene, and syringyl. A sharp transmittance peak between 895 and 900 cm^{-1}, indicative of C–O–C stretching, was observed in all the biomass samples. The peak at 905 cm^{-1} corresponds to glycosidic linkages between sugar units [34].

2.3. Effect of Pretreatment on Calorific Value, Proximal and Ultimate Characteristics

It can be seen in Figure 3a that a higher calorific value was observed in pretreated samples when increasing the SF. The above results demonstrated that increased SF in LHW pretreatment leads to a higher calorific value, attributed to the increase in insoluble lignin microparticulates. The maximum calorific value (27.30 $\pm$ 0.31 MJ kg^{-1}) was at 240 °C for 60 min. It is well known that lignin contributes to a high calorific value in lignocellulosic biomass [35]. Thus, these findings provide evidence that the coalescence of lignin on the surface of pretreated samples affects the calorific properties of PMP. This behavior is particularly pronounced for S_{200}, S_{220}, and S_{240} pretreated samples, pointing towards a preferential formation of complex polymer, as was also confirmed by the thermal and SEM analysis.

Figure 3b shows the ternary diagram of fixed carbon, ash, and volatile matter contents for the native and pretreated samples at different SF of 2.37 to 5.90. Regarding fixed carbon content, the S_{240} sample showed the highest value (39.66 $\pm$ 0.71%), indicating improved fuel properties after LHW pretreatment.. In addition, considering ash's role in enzymatic hydrolysis, the low ash content (2.87 $\pm$ 0.00 wt%) at optimum condition (S_{160}) holds great importance for its potential conversion into fermentable sugars [36]. Interestingly, a low volatile matter content (54.70 $\pm$ 0.59 wt%) was observed in S_{240}, ascribed to pseudo lignin formation.

In general, Van Krevelen plots have been used to display the atomic ratios of H/C and O/C and illustrate a thermal conversion process [37]. These Van Krevelen plots illustrate the impact of the SF of LHW on the H/C and O/C ratios of the raw material and pretreated samples (Figure 3c). We found significant changes in the pretreated samples' elemental composition reflected in the inverse relationships between H/C and O/C atomic ratios and SF. For instance, according to Figure 3c, the raw material showed higher H/C values than the pretreated samples with an SF of 5.90. These results confirm that the lignocellulosic composition, particularly the content of cellulose and hemicellulose, is associated with the H/C and O/C atomic ratios. It has been reported that cellulose and hemicellulose have higher H/C and O/C ratios compared with lignin [37,38]. Therefore, a higher SF results in lower H/C and O/C atomic ratios. Samples with higher lignin content exhibit lower H/C and O/C ratios. Consequently, these samples have higher HHV, which is in agreement with the literature [39].

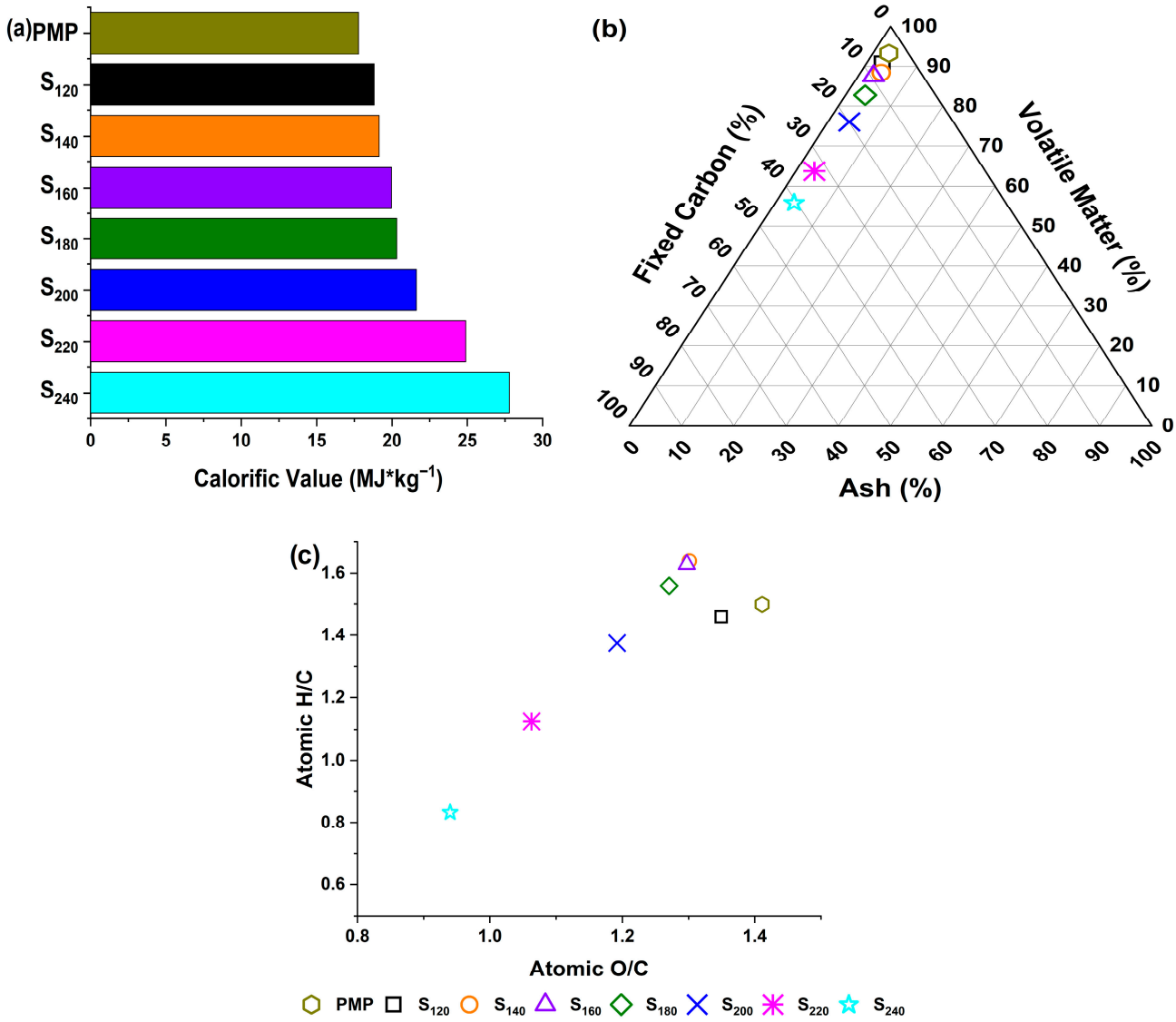


Figure 3. (**a**) Calorific value of native and pretreated samples. (**b**) Ternary diagram for fixed carbon, ash, and volatile matter contents of native and pretreated samples. (**c**) Van Krevelen diagram for native samples and LHW pretreated samples.

2.4. XRD Analysis

Cellulose crystallinity has been intensively investigated owing to it being a key factor in evaluating the efficiency of the enzymatic conversion of cellulosic biomass into renewable biofuels [40–43]. Crystallinity measurements vary among the pretreatments applied to the biomass due to their chemical composition [44]. To investigate the crystallinity changes in the residues after treatments, XRD analysis was used to analyze the crystallinity indexes (CrI) of the native and the treated samples.

The X-ray diffractogram and changes in the CrI of native and different pretreated PMP samples are illustrated in Figure 4 and Table 3, respectively. As can be seen, native cellulose I was observed in the XRD patterns in all samples. Cellulose I is recognized to be composed of two allomorphs, Iα and Iβ. Cellulose Iβ is the dominant polymorph in higher plants [8,45,46]. The diffraction planes of cellulose Iβ (101), (002), and (040) at around $2\theta = 16.00°$, 21.90°, and 34.64° were seen in X-ray diffraction [47]. It has been demonstrated that CrI is significantly correlated with enzymatic digestibility [48]. Moreover, the increase in CrI during pretreatment could result in as good enzymatic digestibility, which can be attributed to the greater enzyme affinity [49]. The S_{160} sample exhibited a higher CrI of

63.99% than the pristine one, with a CrI of 27.20%. The increase in SF from 2.36 to 5.31 after LHW pretreatment indicates the increase in the crystallinity index (CrI) due to the removal of amorphous regions (such as hemicelluloses and lignin) and the degradation of amophous regions of cellulose [44,50–52]. However, the CrI also reduced to 20.35% as the SF advanced to 5.90. The redeposition of degradation products may increase the amorphous content, thereby reducing the CrI of the pretreated sample. The samples with high SF (4.72 to 5.90) showed an amorphous structure, which can be tentatively attributed to the high content of the amorphous phase signal of LCBs.

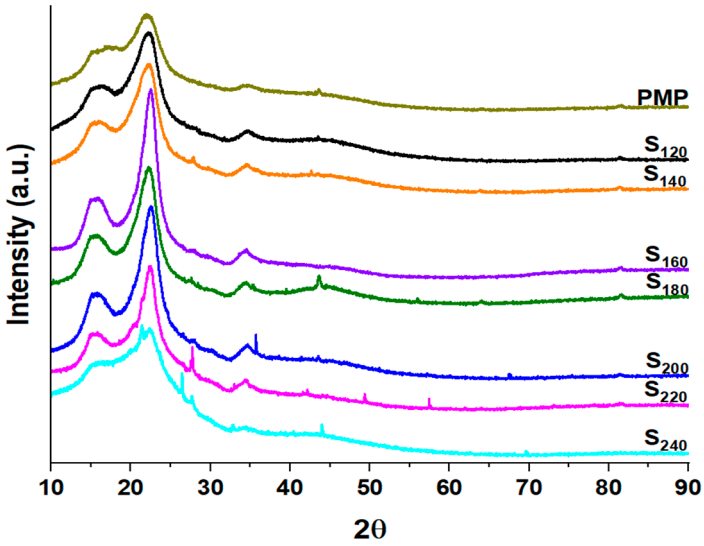


Figure 4. XRD patterns of the raw PMP and the samples pretreated in different SF.

The crystal size of the untreated and pretreated samples was characterized by taking the full-width-at-half-maximum (FWHM) of the (200) lattice plane. Accordingly, the dimension increased from 2.06 nm for the untreated sample to 3.00 nm in the case of the treated samples (Table 3). However, when SF reached 4.72, the crystal size decreased; this observation was tentatively attributed to chemical/mechanical fragmentation during LHW pretreatment, which results in the redeposition of particles with smaller crystalline domains and the rearrangement of crystals. These results indicate that LHW pretreatment can increase cellulose crystallinity and the grain size, with the SF of 3.55 producing the most significant improvement for cellulose conversion rate.

Table 3. Crystallinity index of the residue solids after LHW pretreatment and the native sample.

Sample	CrI (%)	Crystal Size (nm)
PMP	27.20	2.06
S_{120}	35.90	2.30
S_{140}	40.60	2.14
S_{160}	63.99	2.14
S_{180}	47.66	3.09
S_{200}	53.68	2.49
S_{220}	45.47	2.64
S_{240}	20.35	3.00

2.5. TGA

In parallel with the chemical composition analysis, TGA is equally useful for monitoring the physicochemical changes in the biomass sample after pretreatment. Thermal stability of the LHW-pretreated samples was evaluated under a N_2 atmosphere at a range of

20 to 900 °C and a rate of 10 °C min^{-1} compared to cellulose, xylose, and lignin. TG/DTG profiles indicate that the overall structural integrity of PMP shows substantial changes after the LHW pretreatment (Figures 5 and 6). Thermograms also provide remarkable differences in DTG peak temperature and production of char residue (%) of untreated over treated samples (Figure 6). The first zone was observed between 25 and 200 °C, which corresponded to the moisture vaporization. A second zone (about 200–500 °C) comprising the liberation of volatile hydrocarbons from the thermal decomposition of cellulose, hemicellulose, and lignin was observed, being more remarkable in the S_{160} sample, because it was the pretreated sample with the highest cellulose content, compared to pretreated samples. The third zone (≥500 °C) is reponsible for a gradual decrease in weight, which is related to lignin degradation and char formation.

As can be seen in Figure 6, the DTG peaks are maximized at an SF of 4.13, in line with the cellulose content, compared to other samples. The resulting solid residues of LHW treatment show a significant loss of hemicellulose peaks. Importantly, the higher mass weight loss DTG peak (337 °C) is essentially dependent of the remotion of hemicellulose and lignin by the LHW pretreatment. It reflects the potential feedstock that could be converted into fermentable sugars. Pretreated samples under lower SF (2.36 to 4.13) and cellulose exhibited similar TGA profiles, with a remarkable mass loss occurring around 337 °C. Only the pretreated sample with an SF of 5.90 featured two additional peaks at around 365 °C and 453 °C. Additionally, the thermal residue (18.64–36.17% *w*/*w*) was higher for pretreated samples with an SF ranging from 4.72 to 5.90. The weight loss of 20.87% at 500 to 900 °C for PMP treated with an SF of 5.90 was consistent with lignin (18.58%) (Table 4). It has been shown that lignin shares common features with pseudo lignin [53]. One possible explanation for the thermal stability in the temperature range from 500 to 900 °C might be due to changes in the chemical structure as the SF increases. The formation of complex structures, such as pseudo-lignin, likely occurs through the thermal degradation of structural carbohydrates and lignin. With increasing SF, the proportion of condensed polymers (cellulose, hemicellulose, and lignin) in the treated sample increases, making the sample more thermally stable [54]. This has a negative effect on the enzymatic digestibility reaction, thereby decreasing the cellulose conversion yield [55]. Therefore, decreasing the SF of LHW treatment provides a simple strategy for balancing the cellulose content and enhancing the enzymatic accessibility in the PMP as feedstock.

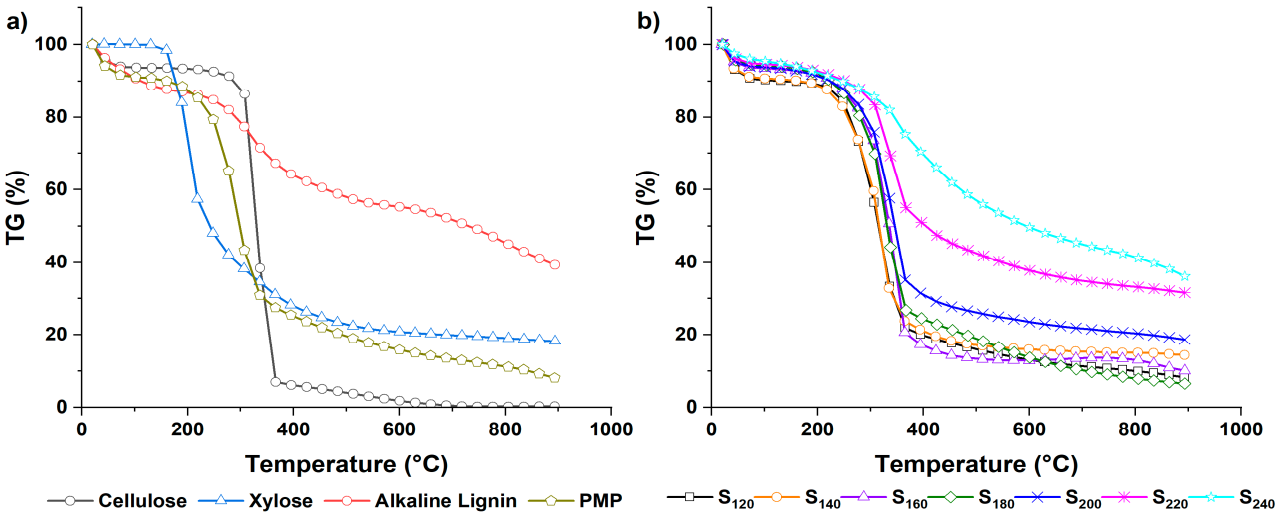


Figure 5. TGA analysis of (**a**) Cellulose, Xylose, Alkaline lignin, and PMP, and (**b**) samples pretreated with different SF at a heating rate of 20 °C/min.

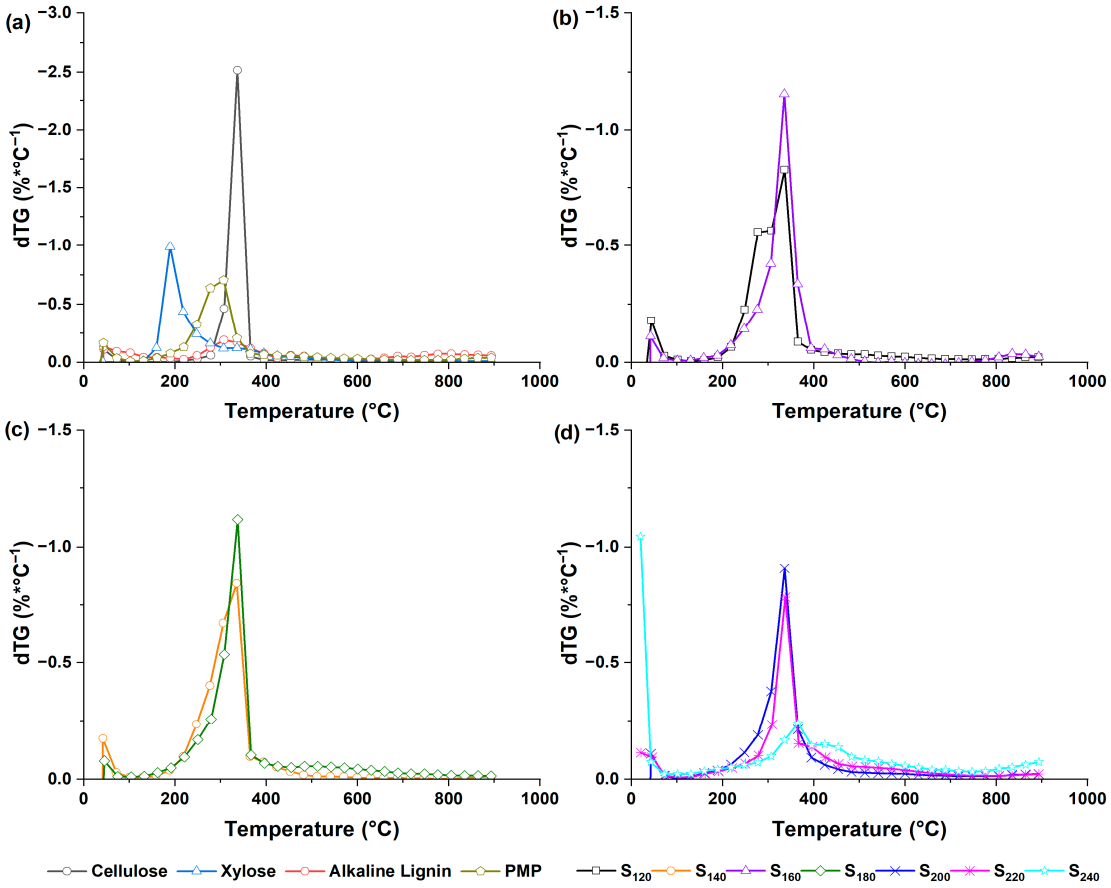


Figure 6. Differential thermogravimetric (DTG) curves of (**a**) individual components: cellulose, xylose, alkaline lignin and PMP; and of pretreated samples: (**b**) S_{120} and S_{160}, (**c**) S_{140} and S_{180}, and (**d**) S_{200} and S_{220}, obtained at a heating rate of 20 °C/min[1].

Table 4. Results of the thermogravimetric measurements—TG curves at 10 °C/min for untreated and pretreated samples.

	First Zone		Second Zone		Third Zone		
Sample	**Temperature Range (°C)**	**Weight Loss (%)**	**Temperature Range (°C)**	**Weight Loss (%)**	**Temperature Range (°C)**	**Weight Loss (%)**	**Residual at 900 °C (%)**
Cellulose	25–200	6.62	200–500	89.31	500–900	3.76	0.31
Xylose	25–200	28.27	200–500	48.95	500–900	4.61	18.16
Alkaline Lignin	25–200	13.17	200–500	28.92	500–900	18.58	39.32
PMP	25–200	12.42	200–500	68.06	500–900	11.42	8.10
S120	25–200	10.83	200–500	73.23	500–900	7.69	8.24
S140	25–200	11.05	200–500	71.85	500–900	2.74	14.35
S160	25–200	8.16	200–500	78.49	500–900	3.29	10.04
S180	25–200	7.95	200–500	73.20	500–900	12.32	6.53
S200	25–200	8.53	200–500	65.35	500–900	7.49	18.64
S220	25–200	7.28	200–500	50.18	500–900	10.94	31.60
S240	25–200	7.61	200–500	35.35	500–900	20.87	36.17

2.6. SEM-EDS Analyses

SEM analysis was used to obtain more insights into the surface morphology and microstructure of native and treated biomass. Figure 7 showcases SEM images for PMP subjected to LHW pretreatment at different SF. The structure of the untreated biomass surface looked like a fibrous network with thick-walled fiber cells, limiting the cellulose accessibility (Figure 7). The SEM analysis revealed that SF levels of 2.36 to 4.15 resulted in solid residues deconstructed with irregular forms of microfibers. This could be related

to the significant degree of delignification, which significantly altered the structure of PMP and decreased their recalcitrance. During the LHW pretreatment, SF led to the fragmentation of lignin, which opened up the compact, packed matrix. However, increasing the SF to 4.72, 5.31, and 5.90 enhanced the formation of spherical droplets and deposited them over copious particles, thus suggesting a redeposition of cellulose, hemicelluse, and lignin products of deconstruction during the LHW pretreatment. These observations are consistent with previous reports [56,57]. It has been reported that deposited lignin droplets on the pretreated substrate's surface restrict enzymatic hydrolysis [15]. Furthermore, the chemical mapping from EDS analysis for the raw and pretreated samples are shown in Figure S1, Supplementary Materials. It was observed that the morphology of the raw sample showed the presence of particles rich in carbon (C), silicon (Si), potassium (K), and oxygen (O). Moreover, it was found that the distribution of C and O in pretreated samples is much higher than the non-pretreated sample. The EDS spectrum revealed that S_{240} had a notably higher C content (68.47%). It corroborates the carbonaceous character already indicated by XRD and TGA.

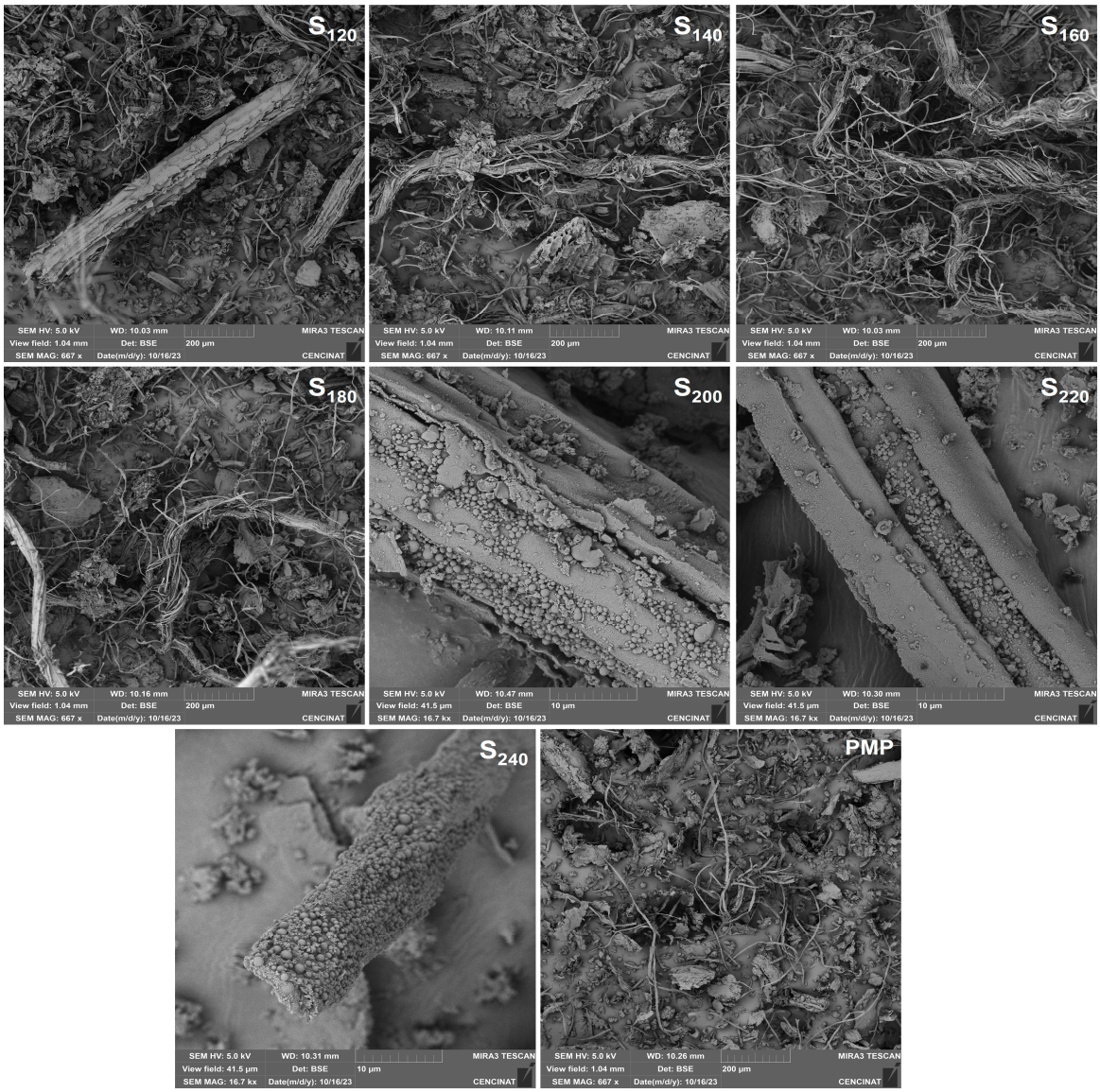


Figure 7. Scanning electron microscope images of untreated and hydrothermal pretreated mother plant pineapple residues.

2.7. Enzyme Hydrolysis

Sustainable use of pineapple biomass requires strategies for efficiently converting complex and recalcitrant natural polymers into renewable chemicals and biofuels. LHW is a fractionation method that provides access to primary components such as cellulose through delignification and hemicellulose removal. The cellulose fraction exists as rigid and semicrystalline fibers that are highly recalcitrant to depolymerization, so deconstruction by cellulolytic enzymes plays a crucial role. For biorefinery applications, thanks to pretreated cellulose, enzymatic conversion has demonstrated superior performance at 20 filter paper units per gram of dry solids [58]. It has been reported that the increase in the enzyme load resulted in significant changes in cellulose conversion [56–58]. The performance of the enzymolysis of native and pretreated samples was investigated with an enzymatic load of 30 filter paper units per gram of dry solids at 50° C during 72 h. Figure 8 presents the profile of glucose release and the cellulose conversion rates during cellulase-catalyzed hydrolysis of pretreated residues compared to raw samples. For PMP samples, LHW pretreatment demonstrated stimulating effects on enzymatic hydrolysis by up to 56.56% compared with raw material. The glucose yield from 38.36 ± 2.96% to 94.92 ± 0.04%, indicating that most of the cellulose is retained in solid residue. Moreover, experiments showed that the processing of PMP results in a significant glucose yield of 0.50 g glucose/g biomass in dry weight when pretreated at 160 °C for 60 min. Compared with the raw material (11.88 ± 0.61 g L^{-1}), the S160 (25.16 ± 0.07 g L^{-1}) demonstrated an overall performance improvement in sugar release. Similar enhancement of enzymatic hydrolysis of pineapple leaves has been reported [59]. However, there was a significant difference in the enzymatic hydrolysis as the SF increased from 4.72 to 5.90; the lignin was compromised by new C-C bonds, referred to as condensation [60–62]. Precise control of lignin condensation is valuable for enzymatic hydrolysis regulation. Moreover, Figure 9 displays a mass balance analysis, which reveals that 21.61 kg of glucose and 1.71 kg of xylose could be generated from 100 kg of raw biomass (dry weight). After LHW pretreatment (S_{160}), only 51.07 kg of treated sample could be recovered from the solid fraction, whereas the liquid fraction had a high xylose content (11.92 kg). Cellulose was mostly present in the solid fraction after LHW pretreatment (25.30 kg). Therefore, LHW significantly removes hemicellulose. These results suggest that LHW could maximize total sugar yield and has the potential to be an alternative pretreatment for PMP biorefinery.

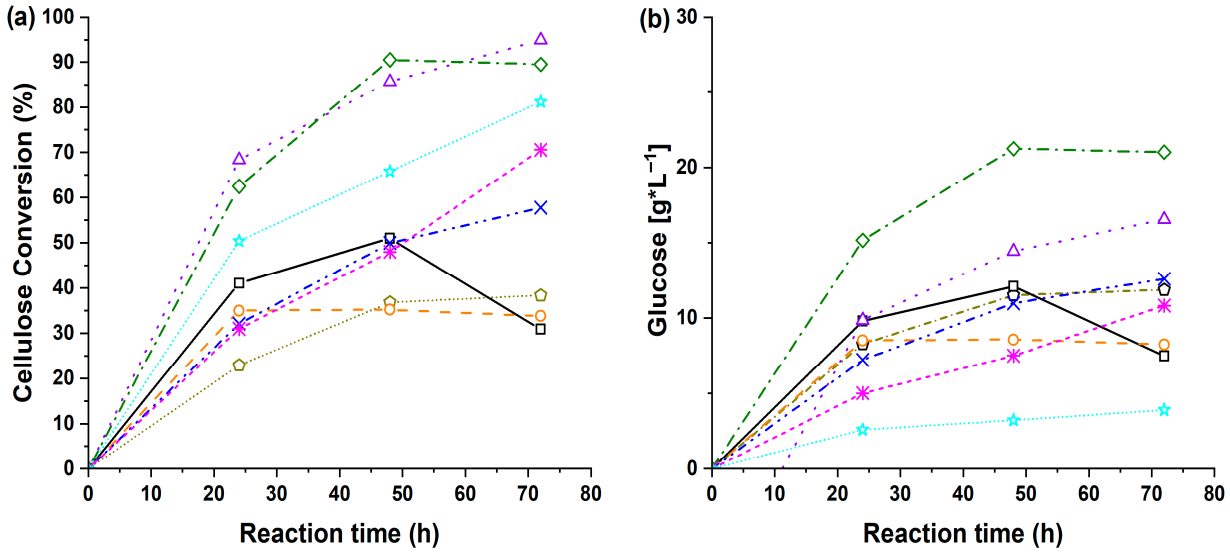


Figure 8. *Cont.*

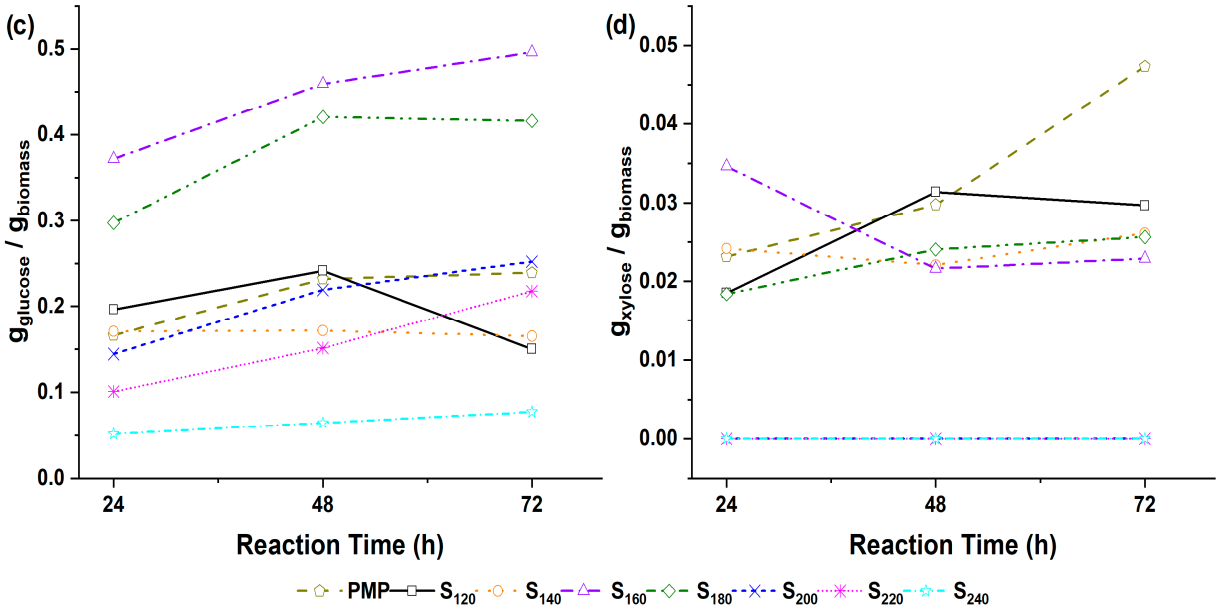


Figure 8. (**a**) Time course of cellulose conversion and (**b**) enzymatic hydrolysis of native and pretreated samples, (**c**) glucose yield and (**d**) xylose yield.

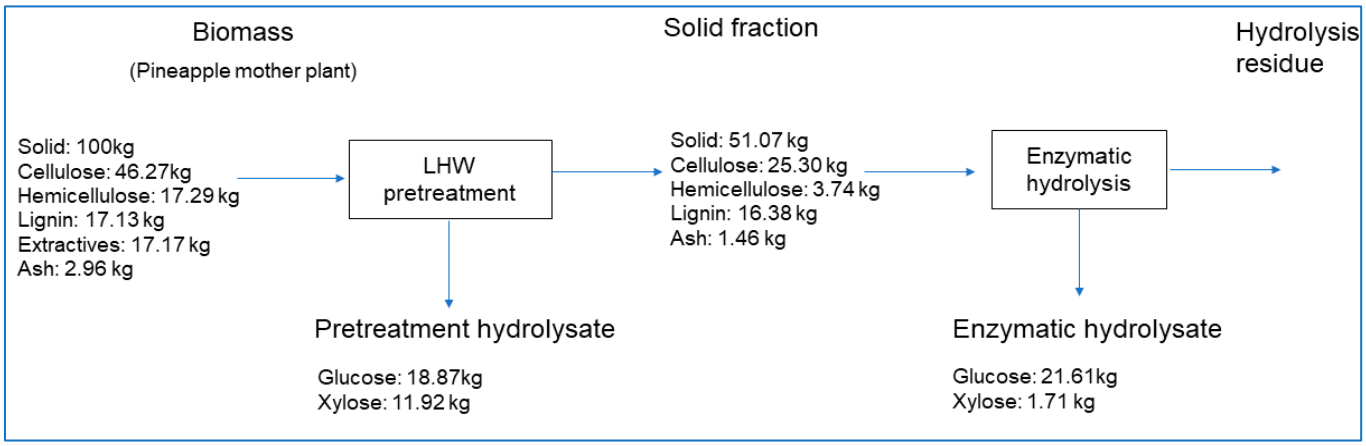


Figure 9. Mass balance of pineapple mother plant biorefinery based on LHW pretreatment to coproduce glucose and xylose.

3. Materials and Methods

3.1. Sample and Pretreatment

Pineapple (Ananas comosus) was kindly supplied by Santo Domingo de los Tsáchilas, Ecuador (00°06.823′ S 079°20.329′ O). The dried pineapple mother plant (PMS), Figure 10, was ground into small powders, and the fraction between 30 and 80 mesh was collected for the hydrothermal pretreatment and enzymatic saccharification studies. Hydrothermal pretreatment was carried out in a floor-standing pressure reactor (Figure 11) with a maximal volume of 3.0 L. For each experiment, the reactor was loaded with 50 g (dry weight basis) of raw PMP suspended in 0.5 L of deionized water, then heated to 120, 140, 160, 180, 200, 220, and 240 °C for a retention time of 60 min. Pretreated samples were labeled as S_{120}, S_{140}, S_{160}, S_{180}, S_{200}, S_{240}, and S_{270}. Temperature was monitored using an inner thermocouple and controlled using a heating/cooling model. In the autohydrolysis process, the reaction media was stirred at 70 Hz. Once the desired operation was reached, the reactor was cooled to about 50 °C by flowing water through an internal stainless-steel loop. The liquid stream and solid residue were separated by filtration with a Whatman filter No. 1, and the

residue was then washed thoroughly with hot water and dried in an oven at 60 °C. The severity factor (*SF*) (Equations (1) and (2)) of the pretreatments based on holding time and temperature was determined as follows [63]:

$$SF = \log R_0 \quad (1)$$

$$R_o = t\ exp\left(\frac{T_r - 100}{14.75}\right) \quad (2)$$

where t is the holding time of pretreatment in minutes, and T_r is the pretreatment temperature in °C.



Figure 10. Pineapple (**a**), Pineapple mother plant (PMP) (**b**), and microphotography of PMP (**c**).

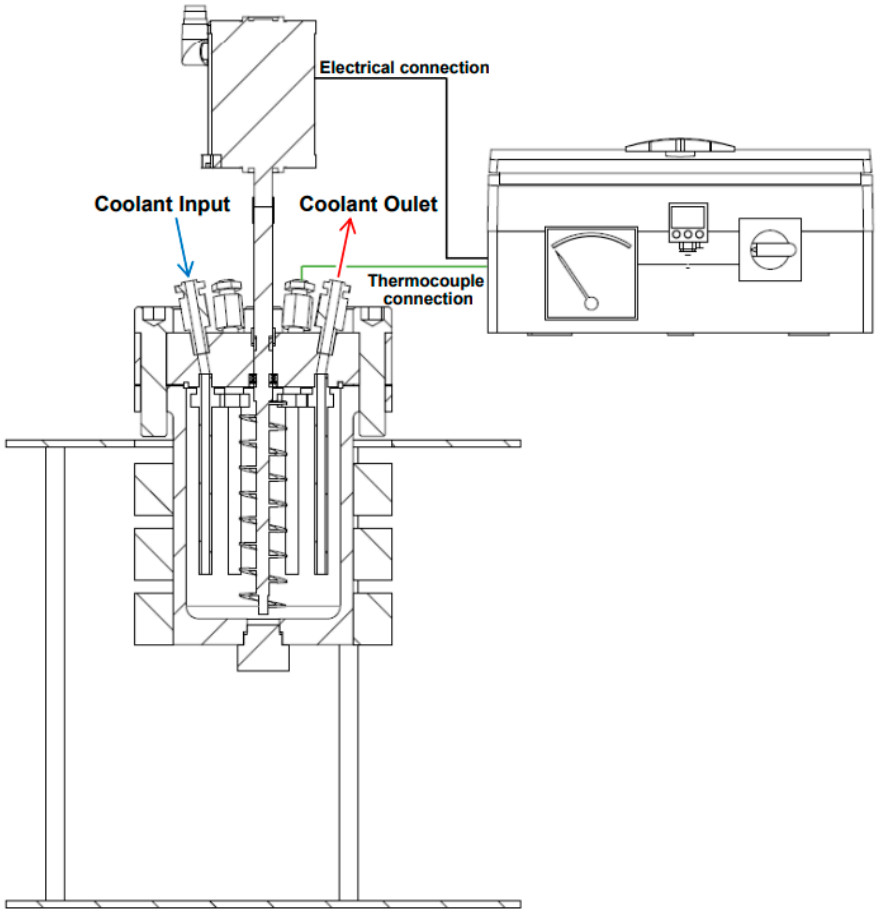


Figure 11. Schematic presentations of the hydrothermal reactor used in this study.

The loss of cellulose and hemicellulose were defined as Equation (3) as follows [64]:

$$SL\ (\%) = 100 \times \left[1 - \frac{y_{i\ final}}{y_{i\ initial}}\right] \quad (3)$$

where $y_{i\ final}$ is the content of cellulose or hemicellulose of pretreated material, and yinitial is the content of cellulose/hemicellulose in the untreated sample. Moreover, the delignification was calculated as follows (Equation (4)) [65]:

$$Delignification\ (\%) = \frac{Initial\ lignin\ content - Lignin\ content\ after\ pretreatment}{Initial\ lignin\ content} \times 100\% \quad (4)$$

3.2. Analysis Methods

3.2.1. Chemical Composition

The NREL/TP-510-42618 [66] standard was adopted to determine the cellulose, hemicellulose, and lignin content. A total of of 0.3 g of the dried sample was poured into a glass test tube and then mixed with 3 mL of 72% H_2SO_4. Following this, the sample was held at 30 °C for 1 h with careful agitation at 10 min intervals to ensure complete hydrolysis. The sample was then treated with 84 mL of distilled water and heated at 121 °C in an autoclave for 1 h. Hydrolysates were filtered, and the solid residue was dried at 105 °C for 12 h to a constant weight. The resulting solid residue corresponds to the acid-insoluble lignin. The filtrate was used to analyze the soluble lignin and determine the carbohydrates. Soluble lignin was estimated using an UV-VIS spectrophotometer (Hach DR600 (Berlin, Germany) at 320 nm. Total lignin was determined as the sum of the acid-soluble and acid-insoluble lignin. Carbohydrates were quantified via HPLC (Agilent 1260 Infinity System, Waldbronn, Germany) with refractive index (RI) detection using a Rezex column (RHM-Monosaccharide H+ 8%, 300 × 7.8 mm, particle size 10 µm) operating at 30 °C with a 5 mM H_2SO_4 solution eluent at 0.5 mL/min flow rate [67].

3.2.2. Extractives Content

Water and ethanol extract content was analyzed according to NREL/TP-510-42619 standard [68]. In a Soxhlet apparatus, 4 g of dried biomass was extracted with 190 mL of ethanol or water and refluxed for 16 h. The residual extract was dried in a hot air oven at 105 °C for 4 h. The extractive content was obtained by weight difference between moisture free biomass and extractive complementary powder.

3.2.3. Proximate Analysis

Proximate analysis of the samples was conducted to estimate moisture, ash, volatile matter, and fixed carbon. The moisture content was obtained according to ASTM standard E1756-01 [69]. Briefly, 4 g of untreated or treated samples were weighed in the crucible and heated in a hot air oven at 105 °C until reaching a constant weight. Then the samples were dried in a desiccator and cooled. The moisture content of the samples can be calculated as follows (Equation (5)):

$$Moisture\ (\%) = 1 - \left(\frac{A - B}{C}\right) \times 100 \quad (5)$$

The ash content was determined in triplicate at 750 °C in a muffle following UNE-EN ISO 18122 [70]. Volatile matter (VM) and fixed carbon (FC) were determined using ISO 18123:2015 standard [71]. The samples were incinerated in a furnace at 900 °C for 7 min. The fixed carbon was calculated using Equation (6),

$$Fixed\ carbon\ (\%) = 100 - moisture\ (\%) - volatile\ matter(\%) - ash(\%) \quad (6)$$

The elemental compositiom of the raw and pretreated samples, specifically their carbon (C), hydrogen (H), nitrogen (N), and sulfur (S) content, was estimated on an elemental analyzer (PerkinElmer 2400, Waltham, MA, USA) according to the guidelines, BS EN 15104:2011 [72]. Oxygen content was calculated by subtracting the total compositions. The ratios O/C and H/C indicate the ratio of atomic O to atomic C, and the ratio of atomic H to atomic C, respectively, which were calculated according to the elemental analysis data. The calorific value of the raw and pretreated samples was determined using a bomb calorimeter (IKA® C2000 basic, Staufen im Breisgau, Germany) according to the BS EN 14918:2009 standard [73]. Briefly, the sample (0.5 g) was placed in a sample holder and then poured into a steel capsule of the calorimetric bomb. Afterward, the bomb was placed in a water bath and filled with oxygen at a pressure of 30 bars.

3.2.4. Vibrational Spectroscopy

FT-IR spectras were recorded on a spectrophotometer equipped with an attenuated total reflectance (ATR-FTIR, Perkin-Elmer Spectrum Two, Shelton, CT, USA) in the range of 400 to 4000 cm^{-1} with a resolution of 4 cm^{-1}.

3.2.5. X-Ray Diffraction (XRD)

XRD patterns were captured by a PANALYTICAL EMPYREAN x-ray diffractometer, equipped with a Cu Kα source (λ = 1.54056 Å), and the diffraction intensity was scanned in the range of 2θ = 5° to 50°. Crystallinity index (CI) of the PMS was calculated following Equation (7) [74]:

$$CrI = 100 \times \left[\left(I_{002} - I_{amorphous} \right) / I_{002} \right] \quad (7)$$

where I_{002} is the intensity of a 2θ = 20 for a crystalline portion (cellulose) and $I_{amorphous}$ is the peak at 2θ = 16.6 is for the amorphous portion (cellulose, hemicellulose, and lignin). The crystallite size was determined by the Scherrer equation (Equation (8)) using the peak full width half maximum (FWHM) of the (200) Bragg peak of the same fit [75].

$$Crystal\ size = \frac{\kappa\lambda}{\beta \cos\theta} \quad (8)$$

where κ is the Scherrer's correction factor (0.94), λ is the wavelength of the incident X-ray radiation (0.1542 nm), β is the peak width of the (200) at FWHM in radians.

3.2.6. Thermal Characterization

Thermogravimetric analysis of both raw and pretreated samples was carried out using a TGA (TGA 55, TA Instruments, New Castle, DE, USA). The samples (about 9–12 mg) were heated from ambient temperature to 900 °C (10 °C min^{-1}) under a nitrogen atmosphere (50 mL min^{-1}).

3.2.7. Scanning Electron Microscope Analysis

The morphological changes in the surface architecture of untreated and pretreated PMP were investigated using scanning electron microscopy (SEM, Mira3 Tescan, Brno, Czech Republic). For the SEM imaging, the samples were attached to metal stubs using a carbon adhesive layer and coated with a thin layer of gold (approximately 20 nm).

3.3. Enzymatic Hydrolysis

Enzymatic hydrolysis experiments of hydrothermal pretreated samples were conducted at a substrate ratio of 5.0% (*w*/*v*) in 50 mM citrate buffer (pH 5.0), under constant stirring at 150 rpm, 50 °C in a shaking incubator (HYSC, Nowon gu, Seoul, Republic of Korea). Commercial cellulase (Cellic Cetec 2, 30 FPU g^{-1} based on the dry weight of

the substrate) provided by Novozymes (Shanghai, China) was used for enzymatic hydrolysis. The hydrolyzates were sampled periodically (0.5 mL) after 0, 24, 48, and 72 h and measured by a high-performance liquid chromatography (HPLC) system (Agilent Technologies, 1260 series, Waldbronn, Germany) equipped with a refractive index detector (Agilent Technologies, G13262A, Waldbronn, Germany). A 10 µL sample was injected on a Rezex RHM-Monosaccharide (H^+, 8%, 300 × 7.8 mm, 10 µm) analytical column and eluted with a mobile phase of 5 mM H_2SO_4 at a flow rate of 0.5 mL min^{-1}. All enzymatic hydrolysis experiments were conducted in duplicate. The cellulose conversion after enzymatic hydrolysis was determined based on Equation (5) [59]:

$$Glucose\ released\ (\%) = \frac{w_{glucose\ after\ EH\ in\ the\ liquid} \times H}{w_{glucose\ in\ pretreated\ solid}} \times 100 \quad (9)$$

where H is the hydrolysis factor, 0.90 for glucose.

4. Conclusions

This study evaluated the effects of liquid hot water (LHW) pretreatment on PMP biomass for biorefinery applications. Among the feedstocks examined, PMP exhibited strong potential for fermentable sugar production. Systematic analysis of the severity factor revealed that the maximum enrichment of cellulose occurred at 160 °C for 1 h. Under these conditions, enzymatic hydrolysis of pretreated PMP yielded 21.61 kg of fermentable sugars per 100 kg of biomass, representing a 2.11-fold increase compared with the untreated material. After 24 h of hydrolysis, more than 65% of glucan was converted into glucose.

Compositional and structural analyses confirmed the effects of LHW pretreatment. TGA, XRD, and FT-IR results demonstrated a substantial reduction in hemicellulose content, associated with its decomposition under treatment. XRD analysis further indicated that both crystallinity index (CrI) and cellulose crystal size were influenced by pretreatment severity. In addition, SEM micrographs revealed a notable increase in surface roughness in pretreated samples compared with native PMP, enhancing enzymatic accessibility.

Overall, these findings highlight PMP as a promising feedstock for the production of fermentable sugars under relatively mild LHW pretreatment conditions, offering a viable pathway for subsequent conversion into value-added biochemicals.

Supplementary Materials: The following supporting information can be downloaded at: https://www.mdpi.com/article/10.3390/recycling10060198/s1, Figure S1: EDS spectrum and elemental mapping of native and pretreated samples.

Author Contributions: Conceptualization: N.M.R.C., C.M.-D., D.C., and P.J.E.-M.; Methodology: N.M.R.C., V.R., P.A.C.-P., and A.D.; Investigation: V.R., N.M.R.C., P.J.E.-M., P.A.C.-P., O.M.R.-N., D.C., and A.D.; Visualization: P.J.E.-M.; Supervision: P.J.E.-M., and V.R.; Writing—original draft: C.M.-D., and P.J.E.-M.; Writing—review and editing: P.A.C.-P., A.D., P.J.E.-M., O.M.R.-N., and C.M.-D. All authors have read and agreed to the published version of the manuscript.

Funding: This work is supported by the Pontificia Universidad Católica del Ecuador (Project: QIPR0027-IBYA103281090) and Agencia Española de Cooperación Internacional para el Desarrollo (AECID).

Data Availability Statement: The data supporting this article have been included as part of the Supplementary Materials.

Acknowledgments: The authors gratefully acknowledge the technical support from Universidad de las Fuerzas Armadas ESPE.

Conflicts of Interest: The authors declare no conflict of interest.

Abbreviations

The following abbreviations are used in this manuscript:

LCB	Lignocellulosic biomass
PMP	Pineapple mother plant
LHW	Liquid hot water
SF	Severity factor
SEM-EDS	Scanning electron microscope energy-Dispersive X-ray Spectroscopy
FTIR	Fourier Transform Infrared Spectroscopy
XRD	X-Ray Diffraction
CrI	Crystallinity index

References

1. Wu, P.; Li, Y.; Zheng, J.-J.; Hosono, N.; Otake, K.; Wang, J.; Liu, Y.; Xia, L.; Jiang, M.; Sakaki, S.; et al. Carbon dioxide capture and efficient fixation in a dynamic porous coordination polymer. *Nat. Commun.* **2019**, *10*, 4362. [CrossRef]
2. Eldahshory, A.I.; Emara, K.; Abd-Elhady, M.S.; Ismail, M.A. Catalytic pyrolysis of waste polypropylene using low-cost natural catalysts. *Sci. Rep.* **2023**, *13*, 11766. [CrossRef] [PubMed]
3. Domec, J.-C.; Smith, D.D.; McCulloh, K.A. A synthesis of the effects of atmospheric carbon dioxide enrichment on plant hydraulics: Implications for whole-plant water use efficiency and resistance to drought. *Plant Cell Environ.* **2017**, *40*, 921–937. [CrossRef] [PubMed]
4. Sethupathy, S.; Morales, G.M.; Li, Y.; Wang, Y.; Jiang, J.; Sun, J.; Zhu, D. Harnessing microbial wealth for lignocellulose biomass valorization through secretomics: A review. *Biotechnol. Biofuels* **2021**, *14*, 154. [CrossRef]
5. Kommedal, E.G.; Angeltveit, C.F.; Klau, L.J.; Ayuso-Fernández, I.; Arstad, B.; Antonsen, S.G.; Stenstrøm, Y.; Ekeberg, D.; Gírio, F.; Carvalheiro, F.; et al. Visible light-exposed lignin facilitates cellulose solubilization by lytic polysaccharide monooxygenases. *Nat. Commun.* **2023**, *14*, 1063. [CrossRef]
6. Deng, W.; Feng, Y.; Fu, J.; Guo, H.; Guo, Y.; Han, B.; Jiang, Z.; Kong, L.; Li, C.; Liu, H.; et al. Catalytic conversion of lignocellulosic biomass into chemicals and fuels. *Green Energy Environ.* **2023**, *8*, 10–114. [CrossRef]
7. Petridis, L.; Smith, J.C. Molecular-level driving forces in lignocellulosic biomass deconstruction for bioenergy. *Nat. Rev. Chem.* **2018**, *2*, 382–389. [CrossRef]
8. Ling, Z.; Chen, S.; Zhang, X.; Takabe, K.; Xu, F. Unraveling variations of crystalline cellulose induced by ionic liquid and their effects on enzymatic hydrolysis. *Sci. Rep.* **2017**, *7*, 10230. [CrossRef]
9. Sun, S.-C.; Sun, D.; Cao, X.-F. Effect of integrated treatment on enhancing the enzymatic hydrolysis of cocksfoot grass and the structural characteristics of co-produced hemicelluloses. *Biotechnol. Biofuels* **2021**, *14*, 88. [CrossRef] [PubMed]
10. Lü, F.; Chai, L.; Shao, L.; He, P. Precise pretreatment of lignocellulose: Relating substrate modification with subsequent hydrolysis and fermentation to products and by-products. *Biotechnol. Biofuels* **2017**, *10*, 88. [CrossRef]
11. Brondi, M.G.; Vasconcellos, V.M.; Giordano, R.C.; Farinas, C.S. Alternative Low-Cost Additives to Improve the Saccharification of Lignocellulosic Biomass. *Appl. Biochem. Biotechnol.* **2019**, *187*, 461–473. [CrossRef]
12. Fang, L.; Lai, C.; Hua, Q.; Wang, P.; Huang, C.; Ling, Z.; Yong, Q. Lignin-associated factors impede enzymatic hydrolysis of hydrothermally pretreated birch and poplar wood. *Ind. Crops Prod.* **2025**, *226*, 120704. [CrossRef]
13. Li, M.-F.; Chen, C.-Z.; Sun, R.-C. Effect of pretreatment severity on the enzymatic hydrolysis of bamboo in hydrothermal deconstruction. *Cellulose* **2014**, *21*, 4105–4117. [CrossRef]
14. Kim, S.M.; Dien, B.S.; Singh, V. Promise of combined hydrothermal/chemical and mechanical refining for pretreatment of woody and herbaceous biomass. *Biotechnol. Biofuels* **2016**, *9*, 97. [CrossRef]
15. Pu, Y.; Hu, F.; Huang, F.; Davison, B.H.; Ragauskas, A.J. Assessing the molecular structure basis for biomass recalcitrance during dilute acid and hydrothermal pretreatments. *Biotechnol. Biofuels* **2013**, *6*, 15. [CrossRef] [PubMed]
16. Mariano, A.P.B.; Unpaprom, Y.; Ponnusamy, V.K.; Ramaraj, R. Bioethanol production from coconut pulp residue using hydrothermal and postalkaline pretreatment. *Int. J. Energy Res.* **2021**, *45*, 8140–8150. [CrossRef]
17. Garrote, G.; Kabel, M.A.; Schols, H.A.; Falqué, E.; Domínguez, H.; Parajó, J.C. Effects of Eucalyptus globulus Wood Autohydrolysis Conditions on the Reaction Products. *J. Agric. Food Chem.* **2007**, *55*, 9006–9013. [CrossRef]
18. Ruan, L.; Wu, H.; Wu, S.; Zhou, L.; Wu, S.; Shang, C. Optimizing the Conditions of Pretreatment and Enzymatic Hydrolysis of Sugarcane Bagasse for Bioethanol Production. *ACS Omega* **2024**, *9*, 29566–29575. [CrossRef]
19. Sukruansuwan, V.; Napathorn, S.C. Use of agro-industrial residue from the canned pineapple industry for polyhydroxybutyrate production by Cupriavidus necator strain A-04. *Biotechnol. Biofuels* **2018**, *11*, 202. [CrossRef] [PubMed]

20. Khoo, P.S.; Rizal, M.A.M.; Hazrati, K.Z.; Aisyah, H.A.; Supian, A.B.M.; Hassan, N.H.; Mahardika, M.; Razman, M.R.; Khan, T.; Sebaey, T.A. Sustainable chemically treated lignocellulosic pineapple leaf fibre-reinforced polymer composites: Mechanical properties, environmental aspects and applications. *Cellulose* **2025**, *32*, 4101–4142. [CrossRef]
21. Saini, R.; Singhania, R.R.; Patel, A.K.; Chen, C.-W.; Piechota, G.; Dong, C.-D. Sustainable production of cellulose and hemicellulose-derived oligosaccharides from pineapple leaves: Impact of hydrothermal pretreatment and controlled enzymatic hydrolysis. *Bioresour. Technol.* **2024**, *398*, 130526. [CrossRef] [PubMed]
22. Yadav, V.K.; Verma, N.; Kardam, S.K.; Pullela, M. Pineapple leaf fiber in polymer composites: Structure, characterization, and applications. *Mater. Chem. Phys. Sustain. Energy* **2025**, *2*, 100011. [CrossRef]
23. Saini, R.; Chen, C.-W.; Patel, A.K.; Saini, J.K.; Dong, C.-D.; Singhania, R.R. Valorization of Pineapple Leaves Waste for the Production of Bioethanol. *Bioengineering* **2022**, *9*, 557. [CrossRef] [PubMed]
24. Zhang, H.; Wang, X.; Chen, Y.; Chen, Q.; Li, S.; Shi, Y.; Cao, S.; Ma, X. Insights into the effect of hydrolysis medium on the holocellulose decomposition, furfural, and pseudo-lignin formation. *Biofuels Bioprod. Biorefin.* **2021**, *15*, 1046–1053. [CrossRef]
25. Schmatz, A.A.; Salazar-Bryam, A.M.; Contiero, J.; Sant'Anna, C.; Brienzo, M. Pseudo-Lignin Content Decreased with Hemicellulose and Lignin Removal, Improving Cellulose Accessibility, and Enzymatic Digestibility. *BioEnergy Res.* **2021**, *14*, 106–121. [CrossRef]
26. Joseph, P.; Ottesen, V.; Opedal, M.T.; Moe, S.T. Morphology of lignin structures on fiber surfaces after organosolv pretreatment. *Biopolymers* **2022**, *113*, e23520. [CrossRef]
27. Araya, F.; Troncoso, E.; Mendonça, R.T.; Freer, J. Condensed lignin structures and re-localization achieved at high severities in autohydrolysis of *Eucalyptus globulus* wood and their relationship with cellulose accessibility. *Biotechnol. Bioeng.* **2015**, *112*, 1783–1791. [CrossRef]
28. Evgenia, E.K. Gladysheva. Liquid Hot Water and Steam Explosion Pretreatment Methods for Cellulosic Raw Materials: A Review. *Polymers.* **2025**, *17*, 1783. [CrossRef]
29. Hu, F.; Jung, S.; Ragauskas, A. Pseudo-lignin formation and its impact on enzymatic hydrolysis. *Bioresour. Technol.* **2012**, *117*, 7–12. [CrossRef]
30. Jimenez-Gutierrez, J.M.; Verlinden, R.A.J.; van der Meer, P.C.; van der Wielen, L.A.M.; Straathof, A.J.J. Liquid Hot Water Pretreatment of Lignocellulosic Biomass at Lab and Pilot Scale. *Processes* **2021**, *9*, 1518. [CrossRef]
31. Ma, L.; Cui, Y.; Cai, R.; Liu, X.; Zhang, C.; Xiao, D. Optimization and evaluation of alkaline potassium permanganate pretreatment of corncob. *Bioresour. Technol.* **2015**, *180*, 1–6. [CrossRef]
32. Onoji, S.E.; Iyuke, S.E.; Igbafe, A.I. *Hevea brasiliensis* (Rubber Seed) Oil: Extraction, Characterization, and Kinetics of Thermo-oxidative Degradation Using Classical Chemical Methods. *Energy Fuels* **2016**, *30*, 10555–10567. [CrossRef]
33. Trilokesh, C.; Uppuluri, K.B. Isolation and characterization of cellulose nanocrystals from jackfruit peel. *Sci. Rep.* **2019**, *9*, 16709. [CrossRef] [PubMed]
34. Oliveira, J.P.D.; Bruni, G.P.; Lima, K.O.; Halal, S.L.M.E.; Rosa, G.S.D.; Dias, A.R.G.; Zavareze, E.D.R. Cellulose fibers extracted from rice and oat husks and their application in hydrogel. *Food Chem.* **2017**, *221*, 153–160. [CrossRef] [PubMed]
35. Demirbaş, A. Relationships between lignin contents and heating values of biomass. *Energy Convers. Manag.* **2001**, *42*, 183–188. [CrossRef]
36. Awoyale, A.A.; Lokhat, D. Experimental determination of the effects of pretreatment on selected Nigerian lignocellulosic biomass in bioethanol production. *Sci. Rep.* **2021**, *11*, 557. [CrossRef]
37. Chen, W.-H.; Lin, B.-J.; Lin, Y.-Y.; Chu, Y.-S.; Ubando, A.T.; Show, P.L.; Ong, H.C.; Chang, J.-S.; Ho, S.-H.; Culaba, A.B.; et al. Progress in biomass torrefaction: Principles, applications and challenges. *Prog. Energy Combust. Sci.* **2021**, *82*, 100887. [CrossRef]
38. Wang, S.; Wang, Y.; Shi, Z.; Sun, K.; Wen, Y.; Niedzwiecki, L.; Pan, R.; Xu, Y.; Zaini, I.N.; Jagodzińska, K.; et al. Van Krevelen diagrams based on machine learning visualize feedstock-product relationships in thermal conversion processes. *Commun. Chem.* **2023**, *6*, 273. [CrossRef]
39. Castro, R.C.A.; Ferreira, I.S.; Roberto, I.C.; Mussatto, S.I. Isolation and physicochemical characterization of different lignin streams generated during the second-generation ethanol production process. *Int. J. Biol. Macromol.* **2019**, *129*, 497–510. [CrossRef]
40. Agarwal, U.P.; Zhu, J.Y.; Ralph, S.A. Enzymatic hydrolysis of loblolly pine: Effects of cellulose crystallinity and delignification. *Holzforschung* **2013**, *67*, 371–377. [CrossRef]
41. Pihlajaniemi, V.; Sipponen, M.H.; Liimatainen, H.; Sirviö, J.A.; Nyyssölä, A.; Laakso, S. Weighing the factors behind enzymatic hydrolyzability of pretreated lignocellulose. *Green Chem.* **2016**, *18*, 1295–1305. [CrossRef]
42. Ye, D.; Rongpipi, S.; Kiemle, S.N.; Barnes, W.J.; Chaves, A.M.; Zhu, C.; Norman, V.A.; Liebman-Peláez, A.; Hexemer, A.; Toney, M.F.; et al. Preferred crystallographic orientation of cellulose in plant primary cell walls. *Nat. Commun.* **2020**, *11*, 4720. [CrossRef]
43. Zhang, Y.; Huang, M.; Su, J.; Hu, H.; Yang, M.; Huang, Z.; Chen, D.; Wu, J.; Feng, Z. Overcoming biomass recalcitrance by synergistic pretreatment of mechanical activation and metal salt for enhancing enzymatic conversion of lignocellulose. *Biotechnol. Biofuels* **2019**, *12*, 12. [CrossRef]

44. Grimaldi, M.P.; Marques, M.P.; Laluce, C.; Cilli, E.M.; Sponchiado, S.R.P. Evaluation of lime and hydrothermal pretreatments for efficient enzymatic hydrolysis of raw sugarcane bagasse. *Biotechnol. Biofuels* **2015**, *8*, 205. [CrossRef]
45. Nam, S.; French, A.D.; Condon, B.D.; Concha, M. Segal crystallinity index revisited by the simulation of X-ray diffraction patterns of cotton cellulose Iβ and cellulose II. *Carbohydr. Polym.* **2016**, *135*, 1–9. [CrossRef] [PubMed]
46. Park, S.; Baker, J.O.; Himmel, M.E.; Parilla, P.A.; Johnson, D.K. Cellulose crystallinity index: Measurement techniques and their impact on interpreting cellulase performance. *Biotechnol. Biofuels* **2010**, *3*, 10. [CrossRef] [PubMed]
47. French, A.D. Idealized powder diffraction patterns for cellulose polymorphs. *Cellulose* **2014**, *21*, 885–896. [CrossRef]
48. Xu, H.; Che, X.; Ding, Y.; Kong, Y.; Li, B.; Tian, W. Effect of crystallinity on pretreatment and enzymatic hydrolysis of lignocellulosic biomass based on multivariate analysis. *Bioresour. Technol.* **2019**, *279*, 271–280. [CrossRef]
49. Fang, C.; Schmidt, J.E.; Cybulska, I.; Brudecki, G.P.; Frankær, C.G.; Thomsen, M.H. Hydrothermal Pretreatment of Date Palm (*Phoenix dactylifera* L.) Leaflets and Rachis to Enhance Enzymatic Digestibility and Bioethanol Potential. *BioMed Res. Int.* **2015**, *2015*, 216454. [CrossRef]
50. Chang, V.S.; Holtzapple, M.T. Fundamental factors affecting biomass enzymatic reactivity. *Appl. Biochem. Biotechnol.* **2000**, *84*, 5–37. [CrossRef]
51. Alvira, P.; Tomás-Pejó, E.; Ballesteros, M.; Negro, M.J. Pretreatment technologies for an efficient bioethanol production process based on enzymatic hydrolysis: A review. *Bioresour. Technol.* **2010**, *101*, 4851–4861. [CrossRef]
52. Lv, Y.; Chen, Z.; Wang, H.; Xiao, Y.; Ling, R.; Gong, M.; Wei, W. Enhancement of glucose production from sugarcane bagasse through an HCl-catalyzed ethylene glycol pretreatment and Tween 80. *Renew. Energy* **2022**, *194*, 495–503. [CrossRef]
53. Martín, C.; Dixit, P.; Momayez, F.; Jönsson, L.J. Hydrothermal Pretreatment of Lignocellulosic Feedstocks to Facilitate Biochemical Conversion. *Front. Bioeng. Biotechnol.* **2022**, *10*, 846592. [CrossRef]
54. Sannigrahi, P.; Kim, D.H.; Jung, S.; Ragauskas, A. Pseudo-lignin and pretreatment chemistry. *Energy Env. Sci.* **2011**, *4*, 1306–1310. [CrossRef]
55. Somnath, D. Shinde; Xianzhi Meng; Rajeev Kumar; Arthur J. Ragauskas. Recent advances in understanding the pseudo-lignin formation in a lignocellulosic biorefinery. *Green Chem.* **2018**, *20*, 2192–2205. [CrossRef]
56. Sun, S.; Wen, J.; Sun, S.; Sun, R.-C. Systematic evaluation of the degraded products evolved from the hydrothermal pretreatment of sweet sorghum stems. *Biotechnol. Biofuels* **2015**, *8*, 37. [CrossRef]
57. Selig, M.J.; Viamajala, S.; Decker, S.R.; Tucker, M.P.; Himmel, M.E.; Vinzant, T.B. Deposition of Lignin Droplets Produced During Dilute Acid Pretreatment of Maize Stems Retards Enzymatic Hydrolysis of Cellulose. *Biotechnol. Prog.* **2007**, *23*, 1333–1339. [CrossRef]
58. Thulluri, C.; Balasubramaniam, R.; Velankar, H.R. Generation of highly amenable cellulose-Iβ via selective delignification of rice straw using a reusable cyclic ether-assisted deep eutectic solvent system. *Sci. Rep.* **2021**, *11*, 1591. [CrossRef] [PubMed]
59. Mund, N.K.; Dash, D.; Mishra, P.; Nayak, N.R. Cellulose solvent–based pretreatment and enzymatic hydrolysis of pineapple leaf waste biomass for efficient release of glucose towards biofuel production. *Biomass Convers. Biorefin.* **2022**, *12*, 4117–4126. [CrossRef]
60. Questell-Santiago, Y.M.; Galkin, M.V.; Barta, K.; Luterbacher, J.S. Stabilization strategies in biomass depolymerization using chemical functionalization. *Nat. Rev. Chem.* **2020**, *4*, 311–330. [CrossRef] [PubMed]
61. Shuai, L.; Amiri, M.T.; Questell-Santiago, Y.M.; Héroguel, F.; Li, Y.; Kim, H.; Meilan, R.; Chapple, C.; Ralph, J.; Luterbacher, J.S. Formaldehyde stabilization facilitates lignin monomer production during biomass depolymerization. *Science* **2016**, *354*, 329–333. [CrossRef] [PubMed]
62. Li, N.; Yan, K.; Rukkijakan, T.; Liang, J.; Liu, Y.; Wang, Z.; Nie, H.; Muangmeesri, S.; Castiella-Ona, G.; Pan, X.; et al. Selective lignin arylation for biomass fractionation and benign bisphenols. *Nature* **2024**, *630*, 381–386. [CrossRef]
63. Ilanidis, D.; Stagge, S.; Jönsson, L.J.; Martín, C. Effects of operational conditions on auto-catalyzed and sulfuric-acid-catalyzed hydrothermal pretreatment of sugarcane bagasse at different severity factor. *Ind. Crops Prod.* **2021**, *159*, 113077. [CrossRef]
64. Batista, G. Effect of severity factor on the hydrothermal pretreatment of sugarcane straw. *Bioresour. Technol.* **2019**, *275*, 321–327. [CrossRef]
65. Kumar, R.; Kumar, N.; Chaudhary, G.; Saini, S.; Singh, C. Development of a Two-Step Hydrothermal Pretreatment for Sugarcane Bagasse Delignification Surpassing Acidic and Chemical Methods. *Waste Biomass Valorization* **2024**, *15*, 4613–4628. [CrossRef]
66. Sluiter, A.; Hames, B.; Ruiz, R.; Scarlata, C.; Sluiter, J.; Templeton, D.; Crocker, D. *Determination of Structural Carbohydrates and Lignin in Biomass*; Technical Report NREL/TP-510-42618; Laboratory Analytical Procedure; National Renewable Energy Laboratory: Applewood, CO, USA, 2008.
67. Méndez-Durazno, C.; Robles Carrillo, N.M.; Ramírez, V.; Chico-Proano, A.; Debut, A.; Espinoza-Montero, P.J. Bioenergy potential from Ecuadorian lignocellulosic biomass: Physicochemical characterization, thermal analysis and pyrolysis kinetics. *Biomass Bioenergy* **2024**, *190*, 107381. [CrossRef]
68. Sluiter, A.; Ruiz, R.; Scarlata, C.; Sluiter, J.; Templeton, D. *Determination of Extractives in Biomass*; Technical Report NREL/TP-510-42619; Laboratory Analytical Procedure; National Renewable Energy Laboratory: Applewood, CO, USA, 2008.

69. *ASTM E1756-01*; Standard Test Method for Determination of Total Solids in Biomass. ASTM International: West Conshohocken, PA, USA, 2010. Available online: https://www.astm.org/e1756-01.html (accessed on 16 October 2025).
70. Solid Biofuels—Determination of Ash Content. 2016. Available online: https://www.une.org/encuentra-tu-norma/busca-tu-norma/norma?c=N0056486 (accessed on 16 October 2025).
71. Solid Biofuels Determination of the Content of Volatile Matter. 2023. Available online: https://www.iso.org/standard/61516.html#:~:text=ISO%2018123%3A2015%20aims%20to,matter%20content%20of%20solid%20biofuels (accessed on 16 October 2025).
72. Solid Biofuels. Determination of Total Content of Carbon, Hydrogen and Nitrogen. Instrumental Methods (British Standard). 2011. Available online: https://webstore.ansi.org/standards/bsi/bsen151042011 (accessed on 16 October 2025).
73. Solid Biofuels. Determination of Calorific Value. 2009. Available online: https://www.document-center.com/standards/show/BS-EN-14918 (accessed on 16 October 2025).
74. Segal, L.; Creely, J.J.; Martin, A.E.; Conrad, C.M. An Empirical Method for Estimating the Degree of Crystallinity of Native Cellulose Using the X-Ray Diffractometer. *Text. Res. J.* **1959**, *29*, 786–794. [CrossRef]
75. Bhunia, A.K.; Mondal, D.; Parui, S.M.; Mondal, A.K. Characterization of a new natural novel lignocellulose fiber resource from the stem of Cyperus platystylis R. Br. *Sci. Rep.* **2023**, *13*, 9699. [CrossRef] [PubMed]

Disclaimer/Publisher's Note: The statements, opinions and data contained in all publications are solely those of the individual author(s) and contributor(s) and not of MDPI and/or the editor(s). MDPI and/or the editor(s) disclaim responsibility for any injury to people or property resulting from any ideas, methods, instructions or products referred to in the content.